Photocycle Populations with Femtosecond Excitation of Crystalline Photoactive Yellow Protein

Christopher D. M. Hutchison[1], Marius Kaucikas[1], Jason Tenboer[2], Christopher Kupitz[2], Keith Moffat[3],Marius Schmidt[2] and Jasper J. van Thor[1]*

[1] Imperial College London, Molecular Biophysics, South Kensington Campus, Sir Ernst Chain bld, SW7 2AZ, London, UK

[2]University of Wisconsin-Milwaukee, Physics Department, 3135 North Maryland Avenue, Milwaukee, Wi53211, USA

[3]Department of Biochemistry & Molecular Biology and Institute for Biophysical Dynamics,University of Chicago, Chicago, IL60637, USA

* Corresponding author email: j.vanthor@imperial.ac.uktel:+44(0)2075 945071

-Highlights:

Femtosecond pulses at 450 nm create up to 10% photoisomerisation in crystals of the Photoactive Yellow Protein

Effective non-linear cross section associated with S1 is not strongly dependent on pulse duration between 150 fs and 800 fs

Single-shot photobleaching dominates and limits photocycle concentrations for large power density

We investigate photocycle excitation of crystalline photoactive yellow protein using femtosecond laser pulses. This work establishes the feasibility and suitable optical excitation conditions to perform femtosecond time resolved X-ray crystallographic measurements using an X-ray Free Electron Laser. Flash photolysis experiments demonstrated photocycle yields of the long-lived 'pB' signalling state of PYP of up to 10% with pulse durations of 130, 500 and 850 fs at 450 nm wavelength. The power density dependence of the transient pB concentration depends strongly on the pulse duration primarily because photobleaching is prominent at the GW/mm^2 level.

1 Introduction

Femtosecond structural dynamics are traditionally measured using laser spectroscopy methods. It has recently become possible to directly detect ultrafast structural motion with near-atomic resolution and sub-picosecond time resolution[1,2]. Time resolved pump-probe X-ray crystallography measurements conducted at synchrotrons have previously been demonstrated for myoglobin-CO and Photoactive Yellow Protein (PYP) with a time resolution as low as 100 ps[3–9]. X-ray free electron lasers (XFELs) provide femtosecond hard X-ray pulses which can be used for ultrafast protein X-ray crystallography[1,2,10,11]. The serial femtosecond crystallography (SFX) method has emerged as the principal technique to exploit the short pulse duration for pump-probe time resolved crystallography measurements[1,2,12], rather than single-crystal experiments[13]. XFELs such as the Linac Coherent Light Source (LCLS) can provide pulses with a duration as low as 20-80 fs with X-ray energies of 4-10 keV for the fundamental and up to 25 keV for the third harmonic[14]. XFELs possess an inherent temporal

jitter (given as ≈200 fs[15] at LCLS) which previously limited the time resolution that could be achieved by pump-probe schemes with synchronised optical lasers. Recent improvements intiming tools allow higher temporal resolution through accurate measurement of each shot's arrival time followed by time-sorting during processing[16]. This has opened up the possibility to study dynamics of structural changes within protein crystals on previously inaccessible time scales < 1 ps.

In order to successfully detect small photoinduced differences in structure factor amplitudes, it is essential that a significant percentage of the probed crystal volume is photoexcited.In the case of excitation byintense femtosecond optical pulses,optical penetration is dominated by the non-linear cross sections, however populations also have a strong dependence on power density. A further complication is that multi-photonionisation rapidly becomes dominant for most biological molecules, typically in the GW/cm^2 region[17–20], as also shown in this study. The most appropriate optical conditions for a time-resolved X-ray crystallography experiment must therefore be a trade-off between power density and peak power, which establishes hard limits on the experimentally available time resolution and on the maximum levels of detectable populations. Here, we investigate the yields and photobleaching processes in PYP samples in crystalline form, and extract the effective non-linear cross sections.

The maxima of the ground state absorption band of PYP (S_0) is at 449 nm in crystals. Upon single excitation ($S_0 \rightarrow S_1$) from this state PYP can enter into a fully reversible photocycle reaction(shown in Figure 1(a)). The first stage of the photocycle is photoisomerisation of the trans-coumaric acid (pCA) chromophore, which has a time constant reported in the 0.4-1.5 ps range[21,22] and a primary quantum yield approximately 20%[23]. Many femtosecond spectroscopy studies have characterised the primary photochemical reactions of PYP[17,23–31]. Figure 1(b) summarises a scheme of the spectroscopically distinguishable states, adapted from Jung et al.[4]. The rates of excitation, stimulated emission (SE) and excited state absorption (ESA) will dictate the population of S_1. These processes are influenced by the wavelength, duration, spectral phase and power density of the optical pump pulse. This work builds on previous investigations by Lincoln *et al.*[22] into the cross-sections and quantum yields of primary photochemical transitions of PYP in solution. They showed that optimised photo-isomerisation yield with stretched femtosecond pulses has a significant dependence on the pump wavelength within the absorption band. For excitation at 400 nm the yield was limited by multi-photon absorption through excited state absorption (peak at 385 nm). This produces S_2 which can lead to photo-ionisation and the production of a pCA^+ radical and a hydrated electron[17]. The S_2 state has a relatively long recovery time (<1 ms) and will therefore act as a loss of potential photocycle yield population during the time-scales of SFX measurements. Excitation at 490 nm greatly increases the effective SE cross section (2.09×10^{-16} cm^2) resulting in a high level of de-excitation ($S_1 \rightarrow S_0$) that alsolimits the rate of photo-isomerisation[22]. Pumping at 450 nm was found to be the best compromise to minimise both ESA and SE and therefore maximise the population excited to S_1.Additional benefit was found from pulse stretching, however this comes at the expense of pump-probe time resolution. The conversion of S_1 to I_0 is still limited by the quantum yield of ≈20%[22], which sets the absolute maximum yield that could be achieved with short pulses.

Those measurements and spectroscopically distinguishable states were obtained from solution experiments. Although the states are likely to be similar in crystals, the rates for their formation and decay, and hence their peak populations, may differ significantly in crystals and solution, due ultimately to the additional constraints imposed on each molecule in the crystal by the intermolecular contacts. These constraints favour the ground state in which the crystals were grown; and the crystallization medium often has unusual conditions of ionic strength and pH that may further alter the kinetics[32]. Hence, the best compromise in conditions for experiments on

crystals must be determined afresh. In order to perform measurements on crystalline PYP the repetition rate must be reduced to 10 Hz[32], to allow full photocycle ground state relaxation (Figure 1a) if the probe spot is not moved, which we also experimentally confirmed. 1 ms after excitation, the pump-probe difference spectrum shows a fully developed ground state (transient) bleach at 446 nm, and 449nm in crystals[32] and has negligible contribution from the blue-shifted 'pB' state which absorbs maximally at 355 nm[22] and also 355nm in crystals[32]. This has been confirmed to also be the case for crystals of PYP[32], therefore this contribution evaluates the yield of the millisecond intermediate 'pB' that can be achieved by single wavelength flash-photolysis measurements.It follows that a measurement of the ratio of transient absorption at 1ms relative to ground state absorption is a direct and model-free measurement of the fraction of photocycle population. With microsecond delays, TA in the 450-460 nm range corresponds to pG (S_0) and pR states[32–36]. The maximum decrease in absorption at 450-460nm occurs ≈1 ms after the pump pulse[32]. At this delay all molecules in the pR state should have converted to pB or returned to the ground state so the TA signal will measure the pG state depletion. Figure 1(a) shows that in PYP crystals, photocycle channels may lead directly from pR_1 and pR_2 to pG; that is, the photocycle may be short-circuited[32]. The magnitude of the TA signal will therefore under-estimate the population that undergoes photoisomerisation, possibly by as much as half the population present at picosecond delays.Regardless such a TA measurement will give a minimum yield to be expected at shorter timescales under specified pumping conditions. Our aim is to ascertain the pumping conditions that lead to a maximum photocycle yield while minimising non-linear conversions and permanent photobleaching. The effective non-linear cross sections are extracted by fitting to rate equations as done for open-aperture Z-scan measurements[22,37].

Femtosecond pump pulses are generally shorter than the relaxation/recovery time of states and as a result it is not possible for relaxation into re-excitation events to occur during the pulse. The total photocycle yield observed will therefore result from a single excitation event. This is a necessity in preparing a coherently excited population for a time resolved measurement; however, it does mean that the maximum yield is limited by the quantum yield. This contrasts with pumping by, for example, ns pulses[12] which are longer than the relaxation time of the excited state in the case of PYP and multiple re-excitation events can occur enhancing the yield.

2 Methods

2.1 Samples

Photoactive yellow protein was prepared as described elsewhere[38]. Large crystals (1 mm x 0.3 mm x 0.3 mm) were grown at room temperature in sitting drops by the vapour diffusion method. 10 µl of PYP solution (~35 mg/mL in HEPES, pH 7) was mixed with an equal amount of reservoir solution containing 2.7 mol/L Na-malonate pH 7. Crystals appeared after three days and were fully grown after about 2 weeks.Crystals were stored and shipped in Eppendorf tubes in 3 mol/L Na-malonate, pH 7.

The SFX method provides a fresh crystal for each X-ray exposure, achieved by jetting microcrystals into the interaction region[39,40]. Such crystals are typically smaller than 5µm in length[12]. The random orientations of PYP crystals in the jet, the variation in microcrystal dimensions, and the different extinction coefficients associated with the ordinary and extraordinary directions of the uniaxial, hexagonal, crystals suggest that a linearly polarised field will encounter a range of optical densities (OD) between 0.2 and 0.8. Such crystals are not suitable for our spectroscopic measurements as they would require very tight focusing of the pump and probe beams on a single microcrystal. This would result in excessive ground state depletion due to the CW probe (discussed further in

section2.2). The solution was to create crystal `pancakes' by squeezing much larger (≈1 mm long) PYP crystals between two 0.18 mm thick siliconised glass plates[41].This formed a thin layer of randomly oriented crystalline matter with significantly lower OD than the larger crystal but with a much larger footprint. The OD of a `pancake' was dependent on the amount of force used to compress the crystal and its initial size and shape. Data was separated into OD bins of <0.3, 0.3-0.8 and >0.8. Comparisons of the total photocycle recovery time from a single excitation pulsehave shown that these 'pancakes' have recovery times in keeping with single crystals (100ms) and are not like solutions of PYP that recover on a much slow timescale (>1 second).

2.2 Optical set-up

The pump-probe optical set-up is shown in Figure 2. The probe was a 445 nm CW diode laser which was attenuated and spatially filtered to give a 2 µW Gaussian beam. The pump was 450 nm 150 fs laser pulses produced using an OPA (TOPAS, Light Conversion) pumped by an 800 nm CPA Ti:sapphire laser system (Solstice, Spectra Physics) giving up to 3.5 µJ at 450nm at the target. As both the pump and probe were operating at very similar wavelengths, it was important to keep the intensity of the probe low to prevent ground state depletion. This limits the maximum probe power that could be used and required the use of a high gain photo-diode detector. Although necessary, the high gain also amplified noise and introduced the largest source of error in the measurements.

Stretching optics	Pulse duration (fs)	GDD (fs^2)
-	130 ± 10	1500 ± 200
1 x SF10 (3 mm)	500 ± 30	3800 ± 500
2 x SF10 (3 mm)	850 ± 50	6800 ± 800

Table 1. Pump pulse regimes.Pulse duration and Group Delay Dispersion (GDD)were retrieved usingFROG method.

Different durations of the pump pulses were achieved by stretching the 150 fs pulses using SF10 wedges; details of characterisation are shown in section A.1. A reflective neutral density (ND) filter wheel varied the pump pulse energy without excessive temporal stretching. Three different pulse stretching regimes were used (Table 1) with pulses energies of 0.5-3.5 µJ.

Both beams were focused on the crystalline PYP target using an f=-250 mm AR coated lens to give ≈100 µm and ≈90 µm FWHM spot sizes for the pump and probe, respectively. As the target is constantly exposed to the CW probe it will generate excitation, but simple kinetic rate calculations showed that the thermal recovery rate would exceed the excitation rate for this power density, resulting in 2-3% accumulated levels of pB.

The probe was separated from the majority of the pump using a d-mirror and 4f focusing system with a square iris. The signal was measured using an amplified photo-diode (Thorlabs PDA36A) in 70dB mode providing a gain of $2.36x10^6$ V/A. To prevent the weak probe signal from being obscured by residual scatter from the pump pulse, a fast shutter blocked the photo-diode during the pump pulse. The shutter was constructed from a razor blade glued to the actuator of a disassembled hard disk drive, driven by a simple current pulse circuit[37] and providing an opening time of < 0.5 ms.

Since the photocycle ground state recovery time constant in crystalline PYP is ≈20ms[4,30], the pump laser repetition rate was reduced from 1 kHz to 10 Hz using two custom 1:10 chopper wheels. Measurements of the TA signal decay time constant showed that at this repetition rate there was >99.98% recovery before the arrival of the next pump pulse. In contrast, some remaining pB population in crystals were reported at 100 ms[2]. Our analysis shows that in our TA measurements incomplete ground state recovery can be neglected

The transient absorption signal (ΔA/A) is given as:

$$\frac{\Delta A}{A} \quad (1)$$

Where A_1 and A_2 are the absorptions measured 1 ms after excitation and after full photocycle recovery respectively (see Figure A3(a)). In addition to measuring the TA signal, samples were illuminated for ≈200 sequential shots to measure the single shot b leaching (SSB) as a function of pulse energy and duration, which showed a uniform response throughout the pulse series. The SSB is given as, and can additionally be verified from the decay of A_0 (absorption before excitation) in the pulse train:

$$\frac{\Delta A}{A} \quad (2)$$

2.3 Nonlinear cross section determination

Calculations based on theory adapted from open aperture z-scan scan data analysis[37] were made to model the TA photocycle yields. To calculate a total non-linear cross-section (σ_{nl}) factor encompassing all of the effects (SE, ESA, pR recovery etc.) which act to lower the yield of pB from the maximum of 20% given by the quantum yield. Equation (3) describes the change in transmission (I(t)) as function of penetration depth (z):

$$\frac{dI}{dz} \quad (3)$$

the ground state population is given as:

$$N_0 \quad (4)$$

And hence the excited state is:

$$N_1 \quad (5)$$

where F(t) is the integrated flux:

$$F(t) = \int_{t_p} \quad (6)$$

σ is the ground state excitation cross section, taken to be 1.682×10^{-16} cm^{-2} at 450 nm[22]. We assumed that all the population was in the ground state before arrival of the pump pulse, and therefore the initial population density of pG (N_0) in molecules per cm^3 could be calculated from the absorption using Beer-Lambert law. The photocycle yield, and hence the TA signal expressed as ΔA/A,was taken to be the final population of S_1 after the pulse multiplied by the quantum efficiency (20 %).

This all holds as long as the intensity of the pump pulses does not lead to sequential double excitation. For high intensities, excitation to a higher state (S_2) becomes relevant as this will limit the population of S_1. The population of S_2 is given as:

(7)

Due to the loss of population, (5) becomes:

(8)

Therefore (3) becomes:

(9)

Integrating (9) over all z gives the change the total change in transmission and hence it is trivial to calculate

2.4 Nonlinear cross section for photo-bleaching

Additional calculations were made to model the single shot photo-bleaching (SSB) cross section. In this case it was assumed that the SSB arose from excitation to any higher state (S_H), as for example in (7). However, population excited in this way does not recover, and results in a net loss of the ground state population after photocycle recovery. The change in the linear absorption arising from this lost population is the SSB. The populations and pulse propagation were determined in the same way in section 2.3, except that is replaced with photo bleaching cross section (In general as the non-linear cross section includes excitations which lower the TA signal but also thermally recover and do not result in ground state depletion. The linear absorption after recovery taking into account ground state population lost to S_H is:

(10)

Finally, the single shot bleach is given by using (10) to calculate the change in absorption ($A_0 - A_2$) and substituting into (2). While the total number of photons per molecule for our conditions islow, between $2x10^{-3}$ and $8x10^{-5}$, a large amount of ground state excitation occurs due to the high energy density of the femtosecond pulses. Therefore the excited state absorption must also be included when computationally propagating the pulse through the sample.

3 Results and Discussion

The measured TA photocycle yields are shown in Figure 3. It can be clearly seen that photocycle excitation of the PYP crystals is possible with yields of transient pB up to 10% for all OD conditions and pulse lengths. In the < 0.3 OD case, a much larger spread of the yields could be due to the higher uncertainty in measuring percentage changes at low absorption. Each case shows an initial linear dependence of the yield on the energy density which peaks at ≈0.3 mJ/mm^2 and then sharply

decreases at rates that depends on pump pulse length. For an XFEL experiment, an energy density should be used that corresponds to the peak yield before the TA signal (>0.5 mJ/mm^2). This energy density maximises the photocycle yield and limits non-linear effects.

Theoretical TA signals calculated using the model described in section 2.3 were fitted to the TA data, there wasgood agreement between the shape of the calculated curves and the data. The recovered values of and are shown in table 2. We note that minimum values of are larger than the combination of ESA (0.769x10^{-16} cm^2) and SE (0.117x10^{-16} cm^2) cross sections previously measured for PYP in solution[22]. That work also showed small differences in ESA and SE cross sections dependent on pulse length[22]. We do not observe any large differences between 130, 550 and 850 fs in the energy density with regards to of crystalline PYP within the available experimental accuracy, again in contrast to previous solution measurements[22]. It is also possible that in crystals, the kinetics of the dynamic Stokes shift are accelerated compared with solution. The TA results are however consistent with a primary quantum yield of approximately 20%, which is comparable to the yield in solution. Considerable differences are seen when comparing the values of where shorter pulses have a larger cross-sections, in keeping with previous obsevations[23]. However, the magnitude of sequential double excitation is small compared to the dominating nonlinear cross section that will consequently determine the resulting I_0 levels. The increased for shorter pulses results in faster suppression of the TA signal at increasing energy density. The maximum TA signal is seen at ≈0.3 mJ/mm^2 generally for all durations of pump pulses, with larger values seen for the longer pulses (Figure 2).

OD	Pump pulse Length (fs)	(10^{-17}cm^2)		(10^{-19}cm^2)
		max	min	
< 0.3	130 ± 10	8.41	3.82	11.28
0.3 – 0.8	130 ± 10	9.18	5.16	12.62
> 0.8	130 ± 10	8.41	3.85	12.51
< 0.3	500 ± 30	8.41	3.44	4.59
0.3 – 0.8	500 ± 30	10.71	4.97	7.07
> 0.8	500 ± 30	8.40	3.44	6.98
< 0.3	850 ± 40	9.94	6.12	3.80
0.3 – 0.8	850 ± 40	10.32	4.97	2.68
> 0.8	850 ± 40	10.13	6.12	2.68

Table 2. Results of TA fitting, showing the recovered nonlinear transient cross-section (and the sequential double excitation cross section ( ).

The effect of pulse length becomes more evident when considering the SSB data (Figure 4). Short pulses give rise to larger bleaching for a given energy density. Because of this pronounced non-linearity it may also be concluded that contribution to the SSB signal from any residual long lived pB state at 100ms may be neglected[42]. In agreement with this conclusion, no ground state recovery was seen after blocking the 10Hz pulse train. The model in section 2.4 was fitted to the SSB data (see Table 3). As would be expected, the bleaching is at least 2 orders of magnitude smaller than The values of are slightly smaller than those of as expected, but indicative of a high primary quantum yield following double excitation (Tables 2,3).

Finally, the ratio of the photocycle yield to the SSB was examined (Figure 5). This ratio estimates the purity of any photocycle signal that could be measured in a crystallographic experiment. With larger ratios, temporally resolved structural changes could be more convincingly assigned to photoisomerisation. We note that this ratio is expressed relative to the pB population at 1ms, and

therefore the ratio of the picosecond population relative to SSB could be up to two-fold larger[30]. For lower energy densities (0.1 mJ/mm^2), the TA signal is at least 5 times larger than the SSB, while for higher energy densities the SSB becomes comparable to if not greater than the TA. In general, longer pulses are better due to the smaller associated value of While the ratio is higher for lower energy density, the absolute TA will be also be smaller and more difficult to detect; a balance must be struck.

OD	Pulse length (fs)	(10^{-19} cm^2)	Fit RMS (%)
< 0.3	130 ± 10	8.41	0.65
0.3 – 0.8	130 ± 10	8.41	0.85
> 0.8	130 ± 10	8.41	0.41
< 0.3	500 ± 30	6.5	1.68
0.3 – 0.8	500 ± 30	6.5	0.35
> 0.8	500 ± 30	6.5	0.49
< 0.3	850 ± 40	3.06	0.41
0.3 – 0.8	850 ± 40	3.06	1.04
> 0.8	850 ± 40	3.06	0.57

Table 3. Single shot bleach fitting recovered cross-sections. Three different transient bleaching cross-sections (σ_B) were found depending on pulse length. The fit RMS gives the root mean square difference between the fitted bleaching model and the data collected.

4 Conclusions

We have demonstrated that readily detectable photocycle yields (by X-ray crystallography) of crystalline PYP are possible using femtosecond optical pulses. Photocycle yields >5% and up to 10% were observed for 130, 550 and 850 fs pulses, that also avoid undesirable photobleaching. We emphasize that the populations with femtosecond delays may be larger, as flash photolysis measurement does not include ground state recovery within the first millisecond, reported earlier in crystals. Such yields of ≈10% are sufficient to conduct a time-resolved X-ray crystallographic measurement at an XFEL. The yield is limited by non-linear effects which were found to have cross sections between $5.74\text{x}10^{-17}$ -$1.26\text{x}10^{-16}$ cm^2. Single shot bleaching becomes very significant at energy densities greater than 1 mJ/mm^2 and leads to irreversible bleaching of several percent. We determined the best conditions to lie around ≈0.25 mJ/mm^2, which provides the best yield of 5-7% while limiting the effect of bleaching to ≈1%.

In order to prepare detectable levels of photolysed population, the optical parameters must be chosen such that the time resolution is limited by the pulse duration.Additionally, the bandwidth necessarily prepares femtosecond coherence by pumping a sub-set of nuclear coordinates. With the expectation that high-repetition rate TR-SFX at the European XFEL will improve detectable levels, this works also will guide future experiments that use shorter optical pulses to enhance the experimental bandwidth and additionally modify femtosecond coherence amplitudes.

5 Acknowledgements

The work wassupported by EPSRC grant EP/M000192/1 to JJvT and CDMH. MS, JT, CK are supported by NSF-STC “BioXFEL” (NSF-1231306) and NSF-0952643 (MS). KM is supported by NIH grant EY 024363.

6 Bibliography

1. Barends, T. R. M. *et al.* Direct Observation Of Ultrafast Collective Motions In CO Myoglobin

Upon Ligand Dissociation. *Science***350,** 445–50 (2015).

2. Pande, K. *et al.* Femtosecond Structural Dynamics Drives The Trans/Cis Isomerization In Photoactive Yellow Protein. *Submitted to Science*

3. Schotte, F. *et al.* Watching A Signaling Protein Function In Real Time Via 100-ps Time-resolved Laue Crystallography. *Proc. Natl. Acad. Sci. U. S. A.***109,** 19256–61 (2012).

4. Jung, Y. O. *et al.* Volume-conserving Trans–cis Isomerization Pathways In Photoactive Yellow Protein Visualized By Picosecond X-ray Crystallography. *Nat. Chem.***5,** 212–220 (2013).

5. Schotte, F. *et al.* Watching A Protein As It Functions With 150-ps Time-Resolved X-ray Crystallography. *Science***300,** 1944–1947 (2003).

6. Perman, B. *et al.* Energy Transduction On The Nanosecond Time Scale: Early Structural Events In A Xanthopsin Photocycle. *Science***279,** 1946–1950 (1998).

7. Moffat, K. Time-Resolved Crystallography. *Acta Crystallogr. Sect. A Found. Crystallogr.***54,** 833–841 (1998).

8. Ren, Z. *et al.* A Molecular Movie At 1.8 Å Resolution Displays The Photocycle Of Photoactive Yellow Protein, A Eubacterial Blue-Light Receptor, From Nanoseconds To Seconds†. *Biochemistry***40,** 13788–13801 (2001).

9. Ihee, H. *et al.* Visualizing Reaction Pathways In Photoactive Yellow Protein From Nanoseconds To Seconds. *Proc. Natl. Acad. Sci. U. S. A.***102,** 7145–7150 (2005).

10. Chapman, H. N. *et al.* Femtosecond X-ray Protein Nanocrystallography. *Nature***470,** 73–77 (2011).

11. Spence, J. C. H., Weierstall, U. & Chapman, H. N. X-ray Lasers For Structural And Dynamic Biology. *Reports Prog. Phys.***75,** 102601 (2012).

12. Tenboer, J. *et al.* Time-resolved Serial Crystallography Captures High-resolution Intermediates Of Photoactive Yellow Protein. *Science***346,** 1242–6 (2014).

13. Thor, J. J. van *et al.* Signal To Noise Considerations For Single Crystal Femtosecond Time Resolved Crystallography Of The Photoactive Yellow Protein. *Faraday Discuss.***171,** 439–455 (2014).

14. Arthur, J., Materlik, G., Tatchyn, R. & Winick, H. The LCLS: A Fourth Generation Light Source Using The SLAC Linac. *Rev. Sci. Instrum.***66,** 1987–1989 (1995).

15. Chollet, M. *et al.* The X-ray Pump–Probe Instrument At The Linac Coherent Light Source. *J. Synchrotron Radiat.***22,** 503–507 (2015).

16. Harmand, M. *et al.* Achieving Few-femtosecond Time-sorting At Hard X-ray Free-electron Lasers. *Nat. Photonics***7,** 215–218 (2013).

17. Larsen, D. S. *et al.* Incoherent Manipulation Of The Photoactive Yellow Protein Photocycle With Dispersed Pump-Dump-Probe Spectroscopy. *Biophys. J.***87,** 1858–1872 (2004).

18. Larsen, D. S. *et al.* Photoisomerization And Photoionization Of The Photoactive Yellow Protein Chromophore In Solution. *Biophys. J.***86,** 2538–2550 (2004).

19. Franjic, K., Cowan, M. L., Kraemer, D. & Miller, R. J. D. Laser Selective Cutting Of Biological Tissues By Impulsive Heat Deposition Through Ultrafast Vibrational Excitations. *Opt. Express***17,** 22937 (2009).

20. Vogel, A. & Venugopalan, V. Mechanisms Of Pulsed Laser Ablation Of Biological Tissues. *Chem. Rev.***103,** 577–644 (2003).

21. Leslie, A. G. W. The Integration Of Macromolecular Diffraction Data. *Acta Crystallogr. Sect. D Biol. Crystallogr.***62,** 48–57 (2006).

22. Lincoln, C. N., Fitzpatrick, A. E. & Thor, J. J. van. Photoisomerisation Quantum Yield And Non-linear Cross-sections With Femtosecond Excitation Of The Photoactive Yellow Protein. *Phys. Chem. Chem. Phys.***14,** 15752–15764 (2012).

23. Hellingwerf, K. J., Hendriks, J. & Gensch, T. Photoactive Yellow Protein, A New Type Of Photoreceptor Protein: Will This 'Yellow Lab' Bring Us Where We Want To Go?. *J. Phys. Chem. A***107,** 1082–1094 (2003).

24. Vengris, M. *et al.* Contrasting The Excited-State Dynamics Of The Photoactive Yellow Protein Chromophore: Protein Versus Solvent Environments. *Biophys. J.***87,** 1848–1857 (2004).

25. Kennis, J. T. & Groot, M.-L. Ultrafast Spectroscopy Of Biological Photoreceptors. *Curr. Opin. Struct. Biol.***17,** 623–630 (2007).

26. Wilderen, L. J. G. W. van *et al.* Ultrafast Infrared Spectroscopy Reveals A Key Step For Successful Entry Into The Photocycle For Photoactive Yellow Protein. *Proc. Natl. Acad. Sci.***103,** 15050–15055 (2006).

27. Usman, A., Masuhara, H. & Asahi, T. Trans−cis Photoisomerization Of A Photoactive Yellow Protein Model Chromophore In Crystalline Phase. *J. Phys. Chem. B***110,** 20085–20088 (2006).

28. Horst, M. A. van der *et al.* From Primary Photochemistry To Biological Function In The Blue-light Photoreceptors PYP And AppA. *Photochem. Photobiol. Sci.***4,** 688–693 (2005).

29. Joshi, C. P. *et al.* Photoreversal Kinetics Of The I1 And I2 Intermediates In The Photocycle Of Photoactive Yellow Protein By Double Flash Experiments With Variable Time Delay†. *Biochemistry***44,** 656–665 (2005).

30. Nakamura, R., Hamada, N., Ichida, H., Tokunaga, F. & Kanematsu, Y. Transient Vibronic Structure In Ultrafast Fluorescence Spectra Of Photoactive Yellow Protein†. *Photochem. Photobiol.***84,** 937–940 (2008).

31. Devanathan, S. *et al.* Dual Photoactive Species In Glu46Asp And Glu46Ala Mutants Of Photoactive Yellow Protein: A PH-Driven Color Transition. *Biochemistry***38,** 13766–13772 (1999).

32. Yeremenko, S., van Stokkum, I. H. M., Moffat, K. & Hellingwerf, K. J. Influence Of The Crystalline State On Photoinduced Dynamics Of Photoactive Yellow Protein Studied By Ultraviolet-Visible Transient Absorption Spectroscopy. *Biophys. J.***90,** 4224–4235 (2006).

33. Meyer, T. E., Tollin, G., Hazzard, J. H. & Cusanovich, M. A. Photoactive Yellow Protein From The Purple Phototrophic Bacterium, Ectothiorhodospira Halophila. Quantum Yield Of Photobleaching And Effects Of Temperature, Alcohols, Glycerol, And Sucrose On Kinetics Of Photobleaching And Recovery. *Biophys. J.***56,** 559–564 (1989).

34. Meyer, T. E., Yakali, E., Cusanovich, M. A. & Tollin, G. Properties Of A Water-soluble, Yellow Protein Isolated From A Halophilic Phototrophic Bacterium That Has Photochemical Activity Analogous To Sensory Rhodopsin. *Biochemistry***26,** 418–423 (1987).

35. Hoff, W. D. *et al.* Measurement And Global Analysis Of The Absorbance Changes In The Photocycle Of The Photoactive Yellow Protein From Ectothiorhodospira Halophila. *Biophys. J.***67,** 1691–1705 (1994).

36. Hendriks, J., van Stokkum, I. H. M. & Hellingwerf, K. J. Deuterium Isotope Effects In The Photocycle Transitions Of The Photoactive Yellow Protein. *Biophys. J.***84,** 1180–1191 (2003).

37. Wei, T.-H., Huang, T.-H., Lin, H.-D. & Lin, S.-H. Lifetime Determination For High-lying Excited States Using Z Scan. *Appl. Phys. Lett.***67,** 2266–2268 (1995).

38. Borgstahl, G. E. O., Williams, D. R. & Getzoff, E. D. 1.4 .ANG. Structure Of Photoactive Yellow Protein, A Cytosolic Photoreceptor: Unusual Fold, Active Site, And Chromophore. *Biochemistry***34,** 6278–6287 (1995).

39. Weierstall, U., Doak, R. B. & Spence, J. C. H. A Pump-probe XFEL Particle Injector For Hydrated Samples. *arXiv:1105.2104 [physics]* (2011). at <http://arxiv.org/abs/1105.2104>

40. Weierstall, U., Spence, J. C. H. & Doak, R. B. Injector For Scattering Measurements On Fully Solvated Biospecies. *Rev. Sci. Instrum.***83,** 035108 (2012).

41. Purwar, N., Tenboer, J., Tripathi, S. & Schmidt, M. Spectroscopic Studies Of Model Photo-receptors: Validation Of A Nanosecond Time-resolved Micro-spectrophotometer Design Using Photoactive Yellow Protein And??-phycoerythrocyanin. *Int. J. Mol. Sci.***14,** 18881–18898 (2013).

42. Schmidt, M. *et al.* Protein Energy Landscapes Determined By Five-dimensional Crystallography. *Acta Crystallogr. Sect. D Biol. Crystallogr.***69,** 2534–2542 (2013).

A. Appendix

A.1 Frequency resolved optical gating (FROG)

The femtosecond pump pulses were characterised using a custom Second Harmonic Generation Frequency Resolved Optical Gating (SHG-FROG) setupshown in Figure A.1. A beamsplitter was used to split the 450 nm pulse into two replicas which were sent on two independent delay lines. One line had a motorised delay stage to allow a temporal delay (τ) to be introduced. In order to reduce the amount of dispersion introduced by the device itself, the beam-splitter used was a 2μm thick pellicle beam-splitter (Thorlabs BP245B1) and focusing was performed using reflective optics. The replicas were focused into a 20μm substrate mounted BBO crystal cut for SHG ($\Theta = 55^{o}$, $\phi = 90^{o}$). Due to the non-collinear geometry, when the pulses are spatially and temporally overlapped in the crystal an addition SHG signal is visible between the two beams due to momenta cancellation. The resulting 225nm emission $I_{SHG}(\omega,\tau)$ was measured using a UV spectrometer and recorded as a function of relative delay. This FROG signal can be written as:



The signal was analysed using the FROG code software package (J. Wong *et al.*http://frog.gatech.edu/) which creates a theoretical FROG trace from a test pulse and iterates to fit the replicated to the experimental trace in order to fully reconstruct the pulse, including its spectral and temporal phase. The reconstructed pulse is shown in Figure A2.A polynomial fit to the spectral phase within the region of $1/e^2$ of the intensity gives a group velocity dispersion (GVD) and third order dispersion (TOD) of ≈900 $fs^2$and ≈1200 fs^3 respectively for the pulses.

A.2 Transient Absorption Signal

Figure A3(a) shows the transient absorption signal as seen on the amplified photo-diode. The point where the signal was used to calculate the TA signal in Equation (1) is marked. The difference between A_1 and A_2 is the single shot permanent bleaching. Figure A3(b) shows a compressed PYP crystal "pancake" target. The crystal is no longer regularly ordered and can be considered a solid mass of randomly oriented microscopic crystals.

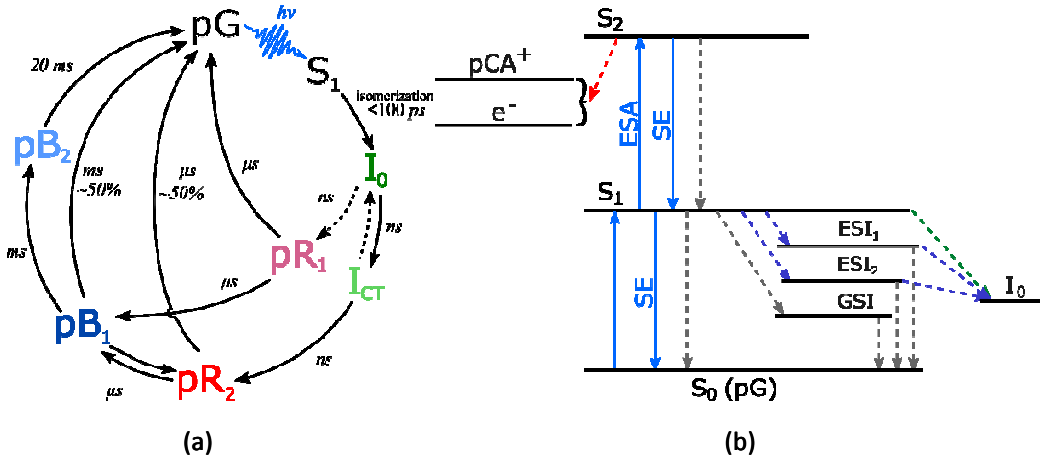


Figure 1. *(a) A kinetic scheme for the photocycle of wild-type PYP in crystalline form showing the more stable intermediates and the time scales between the formations of each. (b) A simplified ground state energy level diagram. Optically driven transitions and relaxation transitions are shown by solid and dashed arrows respectively. Photocycle entry is achieved by relaxation of $S_1 \rightarrow I_0$ either directly (green) or via an excited state intermediate (ESI) (purple). ESA results in double excitation (S_2) which can lead to the photoejection of an electron (e^-) and production of a p-coumaric radical (pCA^+).*

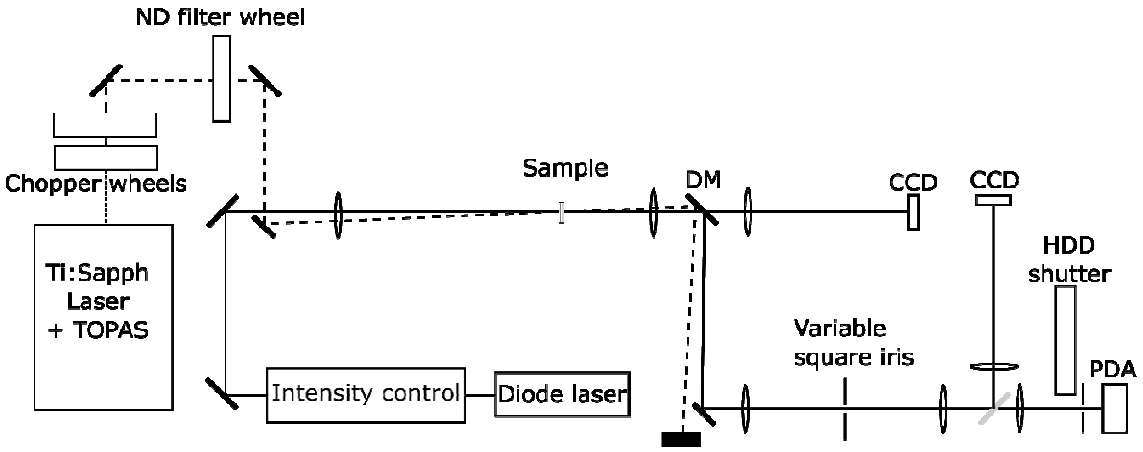


Figure 2. Flash photolysis beam line set-up showing the femtosecond pump (dashed) and CW probe (solid). The probe is recorded on an amplified photo-diode (PDA).

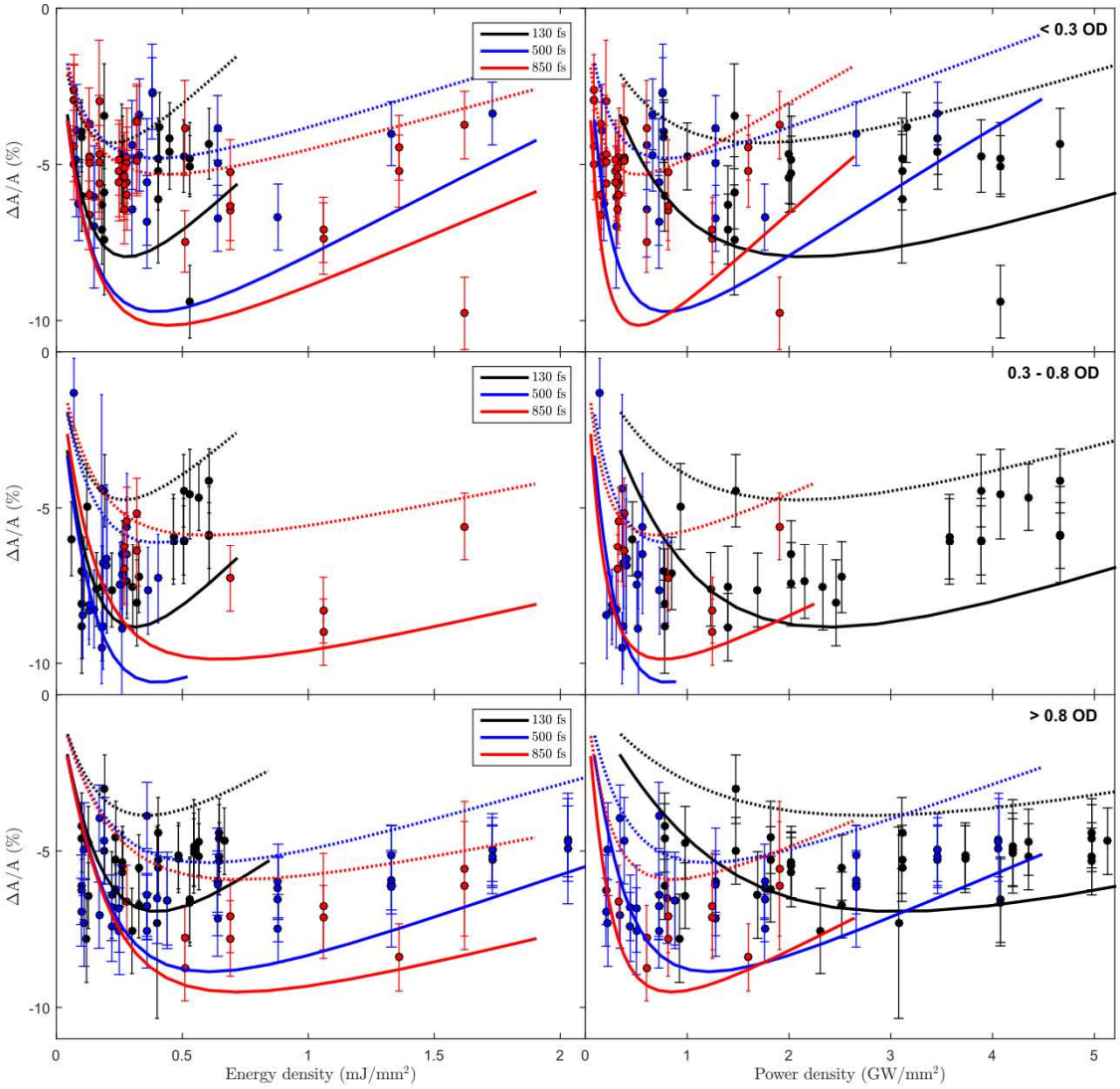


***Figure 3.** Peak TA signals 1 ms after excitation as a function of energy (left column) and power (right column) density. The data is separated into OD's less than 0.3 (top row), between 0.3-0.8 (middle row) and greater than 0.8 (bottom row). Different pump pulse lengths, 130, 550 and 850 fs are shown in black, blue and red respectively. Cross section calculations (section 2.3) have been fitted to the upper (dash) and lower (dash-dot) bounds for the non-linear cross section σ_{nl}. Full details of the fit values are shown in Table 2.*

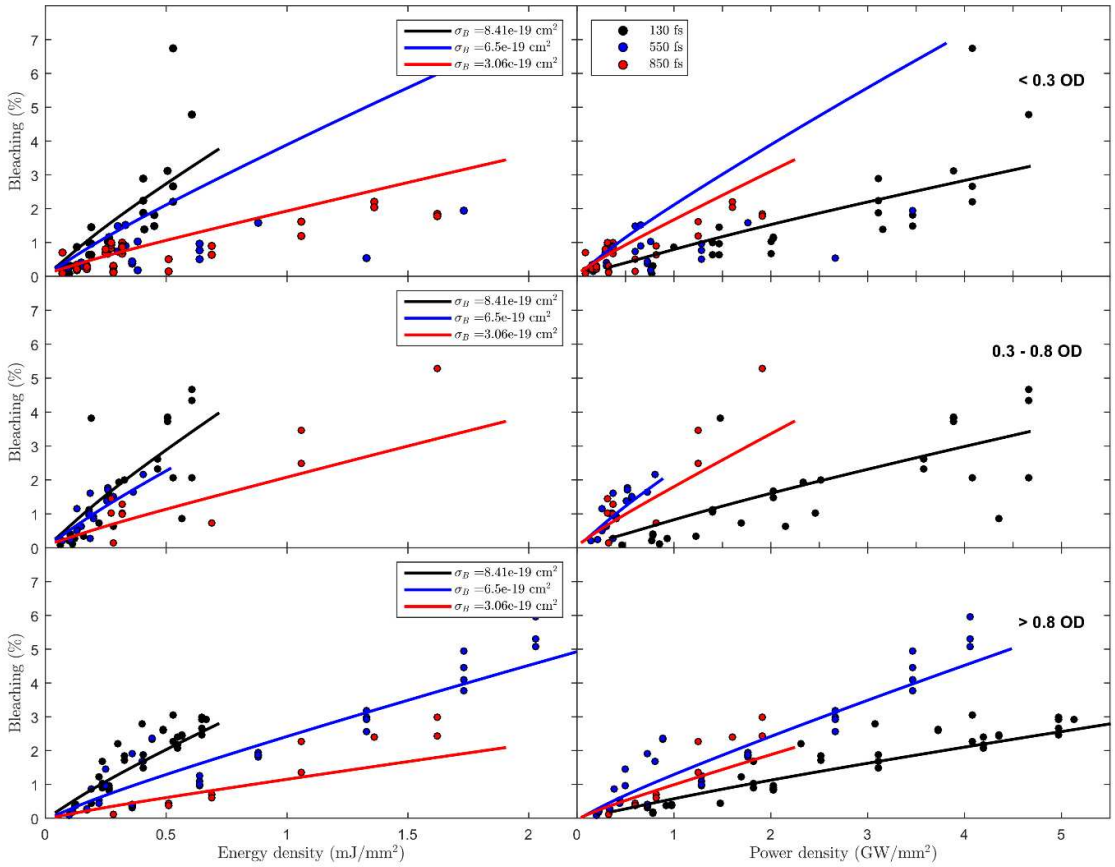


Figure 4. Single shot irreversible bleaching as a function of energy (left column) and power (right column) density for the three different OD regimes. Also shown are the modelled fits (solid line) made using the theory described in section 2.4.

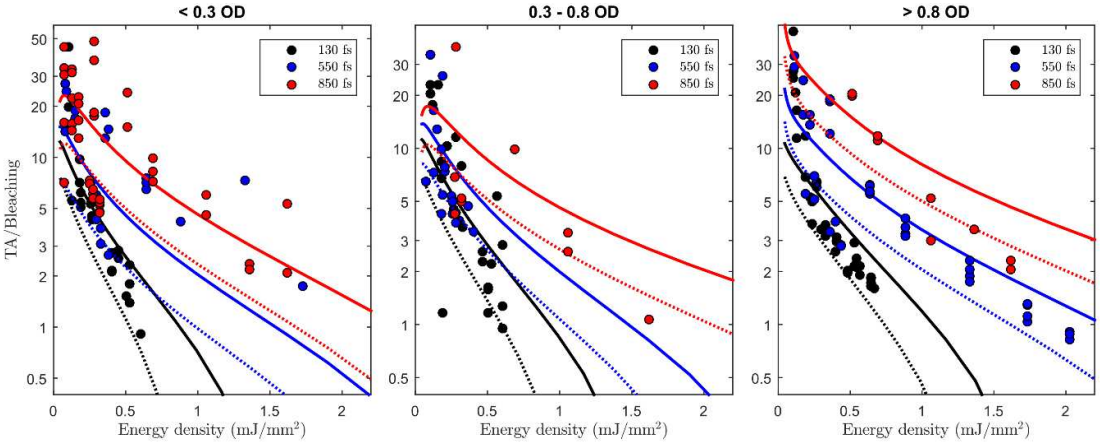


Figure 5. Ratio between the TA signal and the single shot bleaching, for different pulse lengths. Also shown is the ratio of the theoretical fits based on maximum (dashed) and minimum bounds (dash-dot) σ_n from Figure 3.

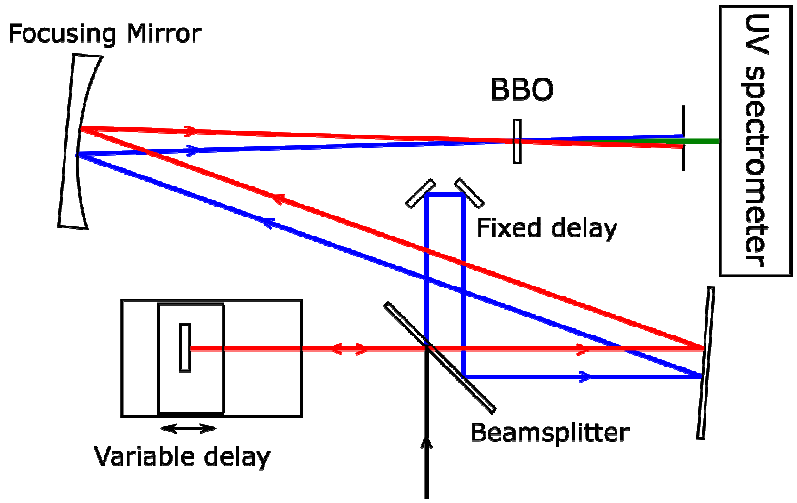


Figure A.1. A schematic diagram of the SHG-FROG setup used to characterise the 450nm pump pulses. The incoming pulse (black) is split into two replicas that travel down individual paths (shown in blue and red for clarity) until they are overlapped in space and time in the BBO crystal. This generates the FROG signal (green) which is measured by the spectrometer.

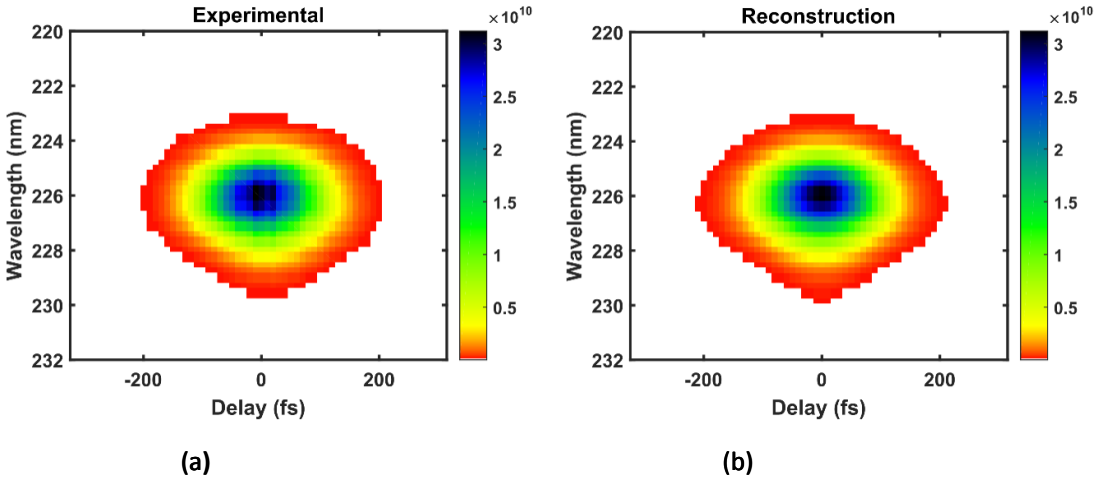
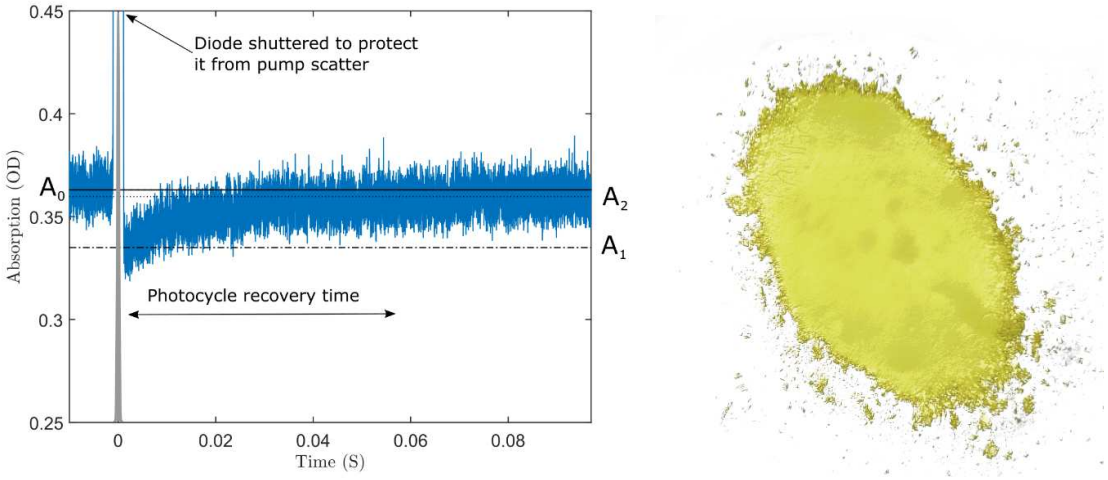


Figure A.2. (a)The experimental and (b) reconstructed FROG traces for the un-stretched 450 nm pump pulse.



(a) (b)

Figure A.3. *(a) An example of a TA signal with various parts of the signal labelled. The pump pulse is shown in grey. (b) Photograph of a typical high OD PYP crystal 'pancake' target (≈1.5 mm long); Low OD pancakes are typically smaller (≈0.5 mm long)*